

Important aspects of investigating optical excitations in semiconductors using a scanning transmission electron microscope

Michael Stöger-Pollach^{1,2}  | Krýstina Bukvišova³ | Keanu Zenz² | Leo Stöger^{2,4} | Ze Scales^{1,5}

¹University Service Center for TEM, TU Wien, Vienna, Austria

²Institute for Solid State Physics, TU Wien, Vienna, Austria

³CEITEC, Bruno, Czech Republic

⁴Atominstytut der TU Wien, Vienna, Austria

⁵KAI Kompetenzzentrum Automobil- und Industrieelektronik GmbH, Villach, Austria

Correspondence

Michael Stöger-Pollach, University Service Center for TEM, TU Wien, 1040 Vienna, Austria.
Email: stoeger@ustem.tuwien.ac.at

Funding information

HORIZON EUROPE European Research Council; Österreichische Forschungsförderungsgesellschaft

Abstract

Since semiconductor structures are becoming smaller and smaller, the examination methods must also take this development into account. Optical methods have long reached their limits here, but small dimensions are also a challenge for electron beam techniques, especially when it comes to determining optical properties. In this paper, electron microscopic methods of investigating optical properties are discussed. Special attention is given to the physical limits and how to deal with them. We will cover electron energy loss spectrometry as well as cathodoluminescence spectrometry. We pay special attention to inelastic delocalisation, radiation damage, the Čerenkov effect, interference effects of optical excitations and higher diffraction orders on a grating analyser for the cathodoluminescence signal.

KEYWORDS

cathodoluminescence, optical properties, scanning transmission electron microscopy, VEELS

1 | INTRODUCTION

Modern electron microscopy is more than just the magnified imaging of small structures. Since the electron beam has sufficient energy, many different processes can be excited in a sample under investigation. Besides ionisation, which can be used for chemical quantification using energy dispersive X-ray spectrometry (EDX) and electron energy loss spectrometry (EELS), the dielectric properties in the optical range can also be investigated. Two techniques are available for this purpose: cathodoluminescence (CL) and valence EELS (VEELS). The optical

range is defined by the wavelength of visible and ultraviolet light, which ranges from approximately 800 to 200 nm. Converted into energy, this corresponds to 1.55–6.2 eV.

Since semiconductor design aims for smaller and smaller structures, analytical techniques have to have an improved spatial resolution. At first glance, the scanning transmission electron microscope (STEM) seems to fulfil these requirements, even if an aberration corrected STEM is employed. Nevertheless, there are some physical limitations in the inelastic electron-matter interaction which have to be dealt with. This work describes some important limits, such as (i) the inelastic delocalisation based on

This is an open access article under the terms of the [Creative Commons Attribution-NonCommercial-NoDerivs](https://creativecommons.org/licenses/by-nc-nd/4.0/) License, which permits use and distribution in any medium, provided the original work is properly cited, the use is non-commercial and no modifications or adaptations are made.

© 2023 The Authors. *Journal of Microscopy* published by John Wiley & Sons Ltd on behalf of Royal Microscopical Society.

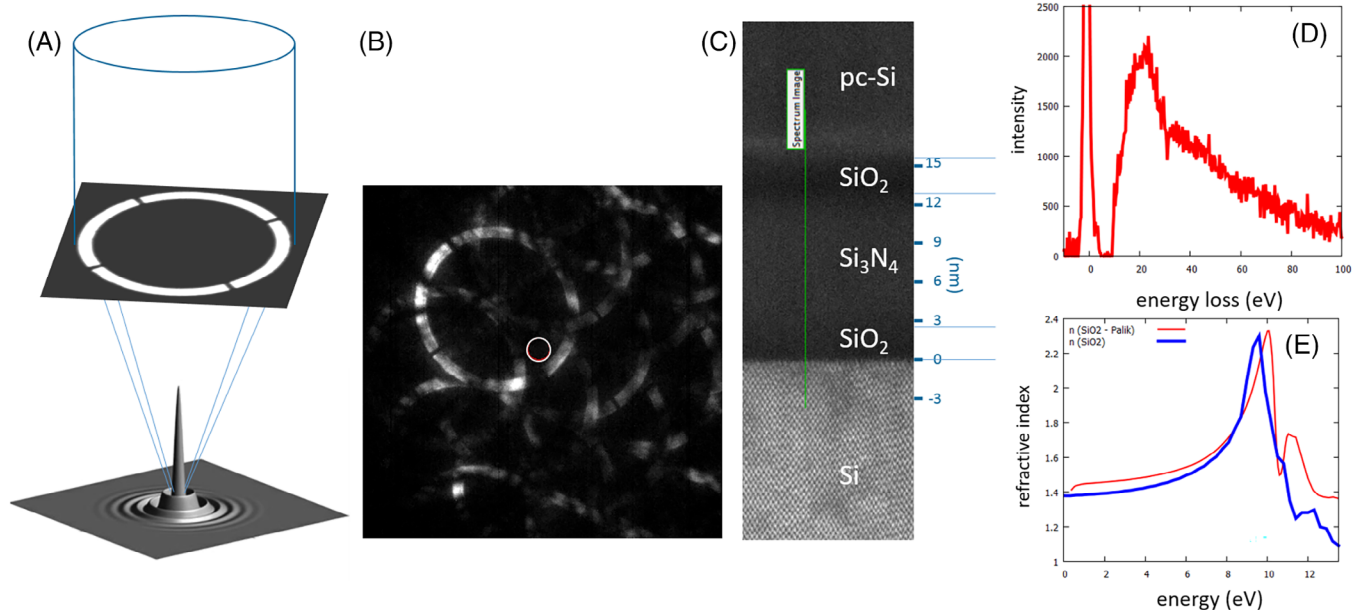


FIGURE 1 (A) Creation of a Bessel beam and its beam profile. (B) Ring-shaped diffraction pattern of Si (110). The white circle shows a possible dark-field position for the EELS measurement. (C) HAADF-STEM image using the Bessel beam of a c-Si/SiO₂/Si₃N₄/SiO₂/pc-Si layer stack of a SONOS transistor. The oxide layer thickness is <3 nm. (D) VEELS spectrum of the lower SiO₂ layer. (E) Refractive index of the SiO₂ layer from employing KKA to the VEELS data in comparison with optical measurements.¹⁴

the long-range Coulomb interaction,^{1,2} (ii) beam damage,³ which must be avoided to study the pristine sample, (iii) Čerenkov photons and losses,^{4–7} which can occur in the optical domain, as well as (iv) their interference at the interfaces of a thin lamella,⁸ and finally (v) diffraction effects of the optical grating spectrometer⁹ must be taken into account in order not to misinterpret the obtained CL results.

The present work is structured as follows: each of the topics (i–v) has its own chapter, in which instructive application examples are given in addition to the theoretical description.

1.1 | Inelastic delocalisation

Inelastic delocalisation was first described already by Niels Bohr in a semiclassical manner.¹⁰ Kohl and Rose¹¹ have used the first Born approximation for calculating the intensity distribution in a plasmon loss image using energy filtered TEM (EFTEM) and find it being dramatically different from the semiclassical limit especially for short distances. Due to the fact that modern STEMs have sub-Å probes, this becomes of more concern as the small probe also suggests high spatial resolution for the EELS measurement.

In general, the long-range Coulomb interaction of the swift electron with the sample causes excitations, even if the electron trajectory passes by the sample, which is called

‘aloof geometry’ in Ref. (1). The strength of this interaction depends on the distance of the trajectory, which is called impact parameter b . In a simple picture, the closer the electron passes by an object, the more energy can be transferred and used for an inelastic scattering event. Even though most publications on inelastic delocalisation deal with aloof geometry, the same picture holds for internal interfaces with an additional restriction: screening of charges inside the medium reduces the impact parameter tremendously. Nonetheless, $b \neq 0$ holds in any case.

A way out of this dilemma is to measure under dark-field conditions.^{2,12,13} Whereas this can be easily achieved using energy filtered high-angle annular dark-field STEM (HAADF-STEM)¹² by employing an in-column filter, with postcolumn energy filters this cannot be done. For this purpose, using a Bessel beam was suggested.¹³ Since a Bessel beam can be created by using a ring-shaped condenser aperture (see Figure 1A), which itself is in a conjugate plane with respect to the back focal plane of the objective lens, a ring-shaped diffraction pattern is projected onto the spectrometer entrance aperture.

Figure 1 shows an example of employing a Bessel beam to a SONOS transistor layer stack. The oxide layers inside the transistor gate have thicknesses below 3 nm and are sandwiching a nitride layer of 9 nm thickness. When the spectrometer entrance aperture is located on a dark-field position in the ring-shaped diffraction pattern (Figure 1B) then the VEELS spectrum (Figure 1D) can be recorded without being influenced by the neighbouring

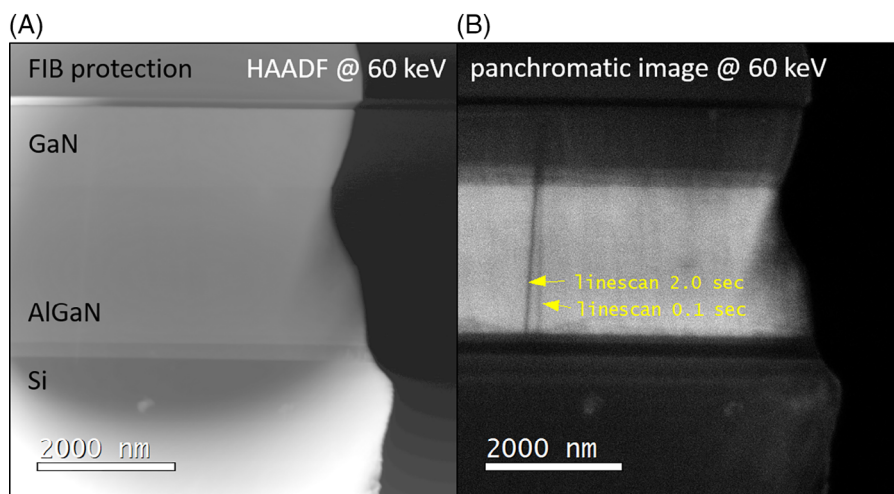


FIGURE 2 (A) 60 keV HAADF image of an AlGaIn/GaN lamella on Silicon. (B) Panchromatic CL image showing the positions of the two line EDX linescans performed at 200 keV beam energy as dark lines.

layers. Without Bessel beams, the neighbouring layers would emit into the spectrometer entrance aperture. Finally, the VEELS data can be used for Kramers–Kronig analysis (KKA) in order to retrieve the refractive index (Figure 1E) and all other optical properties.¹⁵

1.2 | Beam damage

Another critical parameter beside the spatial resolution is the avoidance of beam damage. Since damage alters the optical behaviour of matter, its avoidance is of highest importance. There are two damage mechanisms classified. One of those is the knock-on damage, which increases with increasing beam energy and the other one is radiolysis, which increases with decreasing beam energy. This means that the two mechanisms are opposed. For the improvement of the one, one buys a deterioration of the other. For semiconductors, the knock-on mechanism is the more critical, while for biological samples, radiolysis is more important. ‘Knock-on’ damage does not automatically mean that atoms are knocked out of the sample. It is also sufficient if atoms are displaced in the crystal lattice and migrate to interstitial sites. Thus, point defects are created. They influence the electronic structure of the material and thus its optical properties.

In the case of GaN, fast electrons can create a multitude of such point defects. The damage threshold is around 70 keV.¹⁵ If the optical behaviour is then to be determined by means of cathodoluminescence, the damaged areas of the sample remain dark. Figure 2 shows a GaN lamella that has been examined with 60 keV electrons before two EDX linescans with 200 keV electrons are performed. Afterwards, the light emission at 60 keV was again measured

using CL. The two linescans are clearly visible, whereby the right linescan only had an exposure time of 100 ms per measuring point, while the left scan was recorded with 2000 ms per measuring point.

1.3 | The Čerenkov effect

The Čerenkov effect occurs when fast charges pass through matter at a speed greater than the phase velocity of light in matter. It is common knowledge from classical physics that accelerated charged particles emit electron magnetic waves and that these waves form spherical wave fronts in accordance with Huygens’ principle, which travel at the phase velocity of the medium $c_n = c/n$ (with n being the refractive index of the medium). When a charge carrier passes through a medium, the particles of the medium polarise around it in response. Hence, if $v_{e^-} > c_0/n$ is fulfilled, light is emitted. This limit is called the Čerenkov limit. Employing 200 kV acceleration voltage in the STEM, the speed of the electrons is 69.5% of the vacuum speed of light. Consequently, the Čerenkov effect occurs as soon as the refractive index of the medium is larger than 1.439 and the absorption coefficient is close to zero. Simultaneously with the emission of Čerenkov photons, the electrons responsible for the emission lose energy.

The energy losses are then in the optical range, since photons of the optical light spectrum are generated. As a result, intensities occur in the optical range of the energy loss spectrum that do not depend on the material properties, but merely on the fact that the probe electrons were faster than the phase velocity of light. Although iterative methods exist to mathematically remove these Čerenkov losses in the EELS spectrum, it is advantageous

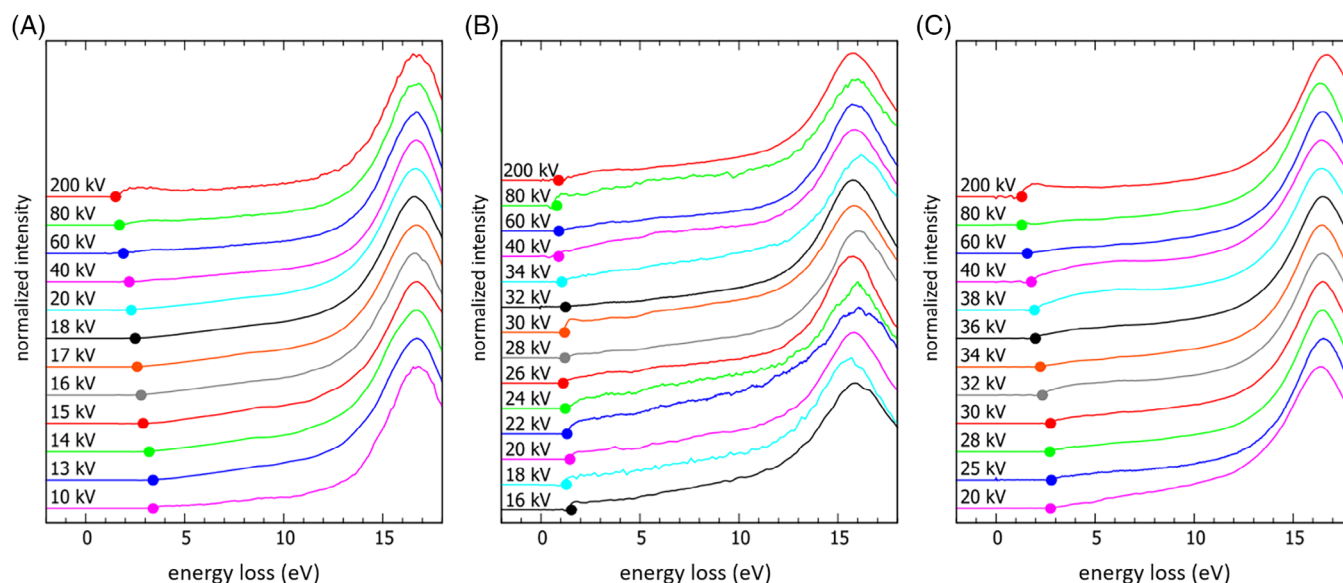


FIGURE 3 VEELS spectra after removal of the ZLP of (A) Si, (B) GaAs and (C) GaP using various beam energies using a nonmonochromated TECNAI TEM. The dot (\bullet) denotes the onset of the inelastic signal. Below the Čerenkov limit, there is no further change of the onset. Redrawn after Ref. (5).

TABLE 1 Refractive indices, direct (d) and indirect (i) bandgaps, Čerenkov limits, and damage threshold for knock-on damage of various semiconductors.

	n (VIS)	Bandgap (eV)	Čerenkov limit (keV)	Damage threshold (keV)
Si	3.98	1.12 (i) / 3.4 (d)	13 ^{5,15}	200 ¹⁷
GaAs	3.94	1.4 (d)	21 ⁵	270 ¹⁸
GaP	3.38	2.2 (i) / 3.03 (d)	30 ⁵	70 ¹⁹
GaN	2.4	3.4 (d)	54 ¹⁵	71 ¹⁶

to avoid them in the first place. As can be seen in Table 1, the Čerenkov limit is in general much lower than the knock-on damage threshold. Therefore, working below the Čerenkov limit automatically means working below the damage threshold, too.

If the VEELS experiment is done utilising beam energies above the Čerenkov limit, the low loss spectrum is altered (as shown in Figure 3). Optical properties cannot be calculated correctly employing KKA except of using an iterative routine as described in an earlier work.²⁰ Even band gap measurements cannot be performed. The onset of the inelastic signal varies with beam energy⁵ and sample thickness.⁴

1.4 | Interference effects in the optical region

When light is excited inside the specimen – might it be by the de-excitation of an electron falling from the

excited conduction state into a hole in the valence band or might it be because of the prior discussed Čerenkov effect – interference can occur if the thickness of the sample is a multiple of half the emitted photon wavelength divided by the respective refractive index of the material (compare Figure 4A). In the case of incoherently emitted photons, which are the ones being related to a de-excitation process, the probability is rather low, since sample thickness and wavelength must fit together. This is rarely the case. In contrast, the coherently emitted photons stemming from the Čerenkov effect show up in a continuous spectrum, thus it is very likely that the sample thickness fits to one of the wave lengths of the Čerenkov spectrum. Hence, interference appears in a prominent manner (see Figure 4B – experiment). Using Yamamoto's equation,²¹ the interference in the CL spectrum can be calculated (see Figure 4B – simulation). The corresponding theory for EELS was developed earlier and can be found in Kröger's main research work.²² Figure 4B and 4 shows an impressive example of interference of the Čerenkov light as well in CL as in EELS with dependence to the sample thickness.

When light is excited inside a medium, it might be partially reflected at the inner sample surfaces, thus being guided for a short distance before being able to leave. Since it is only partial inner reflection, destructive and constructive interference is the consequence, depending on the difference of the path length. The same can be observed in the VEELS spectrum: light guiding modes evolve with sample thickness from a single one to a series of minima and maxima within an energy range starting at the optical gap of 1.12 eV (vertical line in Figure 4C) up to 4.2 eV,

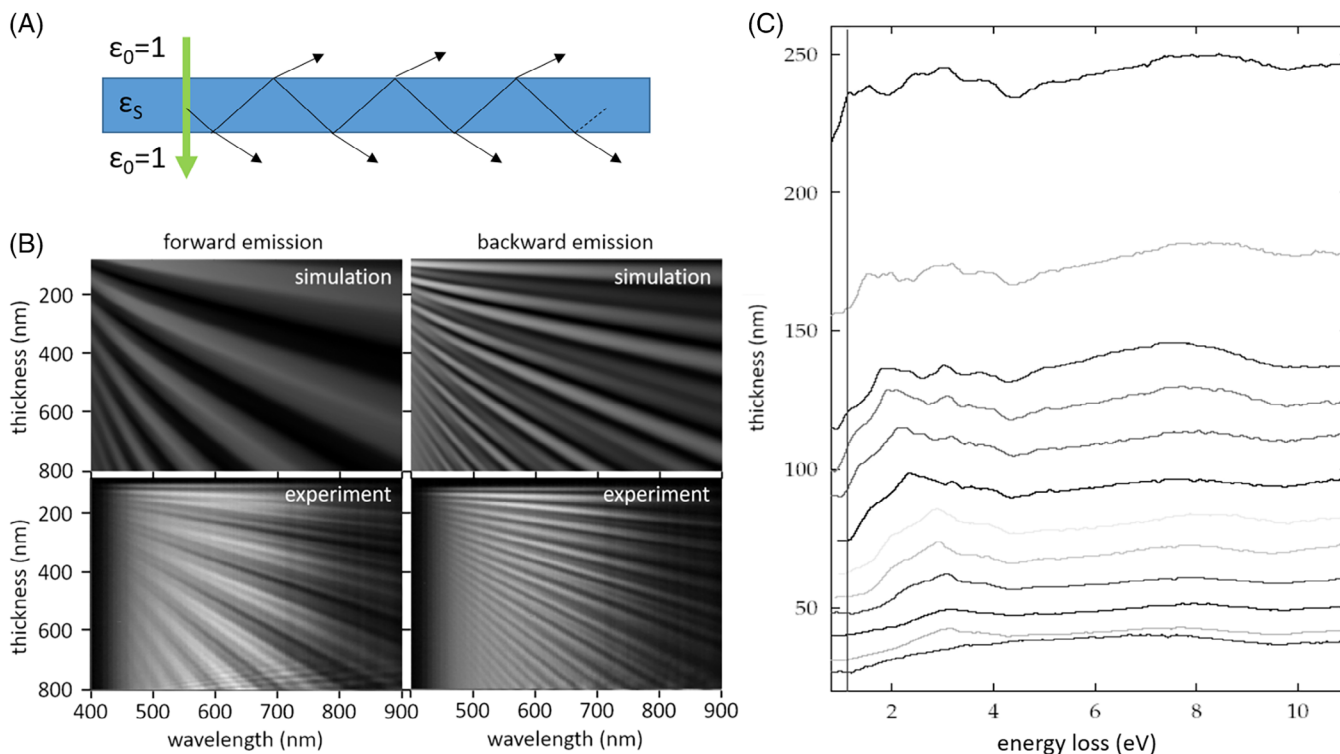


FIGURE 4 (A) Schematics of interference of light inside a specimen. (B) Measured and simulated interference pattern of Čerenkov light in Silicon excited with 200 keV electrons with respect to the sample thickness (y -axis). (C) VEELS spectra of 200 keV electron when passing through Silicon using a monochromated TEM. For better visibility, the spectra are shifted to the respective sample thickness denoted on the y -axis.

where the light is completely absorbed within the thin Silicon slab. The interference pattern might be utilised for the determination of the wavelength dependent refractive index, but has a limited accuracy. VEELS without showing the Čerenkov effect is preferable.⁶

1.5 | Higher-order diffraction in the analysing grid for CL spectroscopy

When analysing light, optical spectrometers are utilised. They can either use a prism or a grating as analysing object. When a prism is used, the disadvantage of a nonlinear spectrum and self-absorption of the optical element has to be taken into account. On the other hand, a grating has the disadvantage of having multiple diffraction maxima, each showing a dispersion of the reflected (or transmitted) light. In order to optimise the reflection grating, blazing was introduced, which is a slight tilt of each mirror plane within a periodic arrangement. With this set-up, the brightest diffraction order can be the first or the second order of diffraction, other orders are suppressed more or less efficiently and also the white zero order of diffraction is weak in terms of intensity. But higher orders are overlapping with the main diffraction order of the respec-

tive grating. In the used experimental set-up, the grating is blazed for the first order and has a blazing wavelength of 500 nm. This means that light having a wavelength of 500 nm is only diffracted into the first order and any multiples of it are totally suppressed. Light having a wavelength of $(500 \pm \delta)$ nm is not fully diffracted into the first order and thus contributes to a measured intensity at n -fold values of the original channel of measurement.²³

Consequently, higher-order diffraction maxima have to be subtracted from a spectrum, if a false interpretation should be avoided. The envelope function on Figure 5A–D is a sinc^2 function. Its width and position depend on the incoming monochromatic light. In the case of polychromatic light the reflection efficiency $\eta_m(\lambda)$ can be described as

$$\eta_m(\lambda) = \text{sinc}^2\left(\frac{\lambda_B}{\lambda} - m\right),$$

where m is the order of diffraction. Consequently, the overall measured spectrum can be written as

$$I(\lambda) = R(\lambda) \cdot e^{-l\alpha(\lambda)} \cdot DQE(\lambda) \cdot \left(\sum_{m=1}^3 I_m(\lambda) \cdot \text{sinc}^2\left(\frac{\lambda_B}{\lambda} - m\right) \right),$$

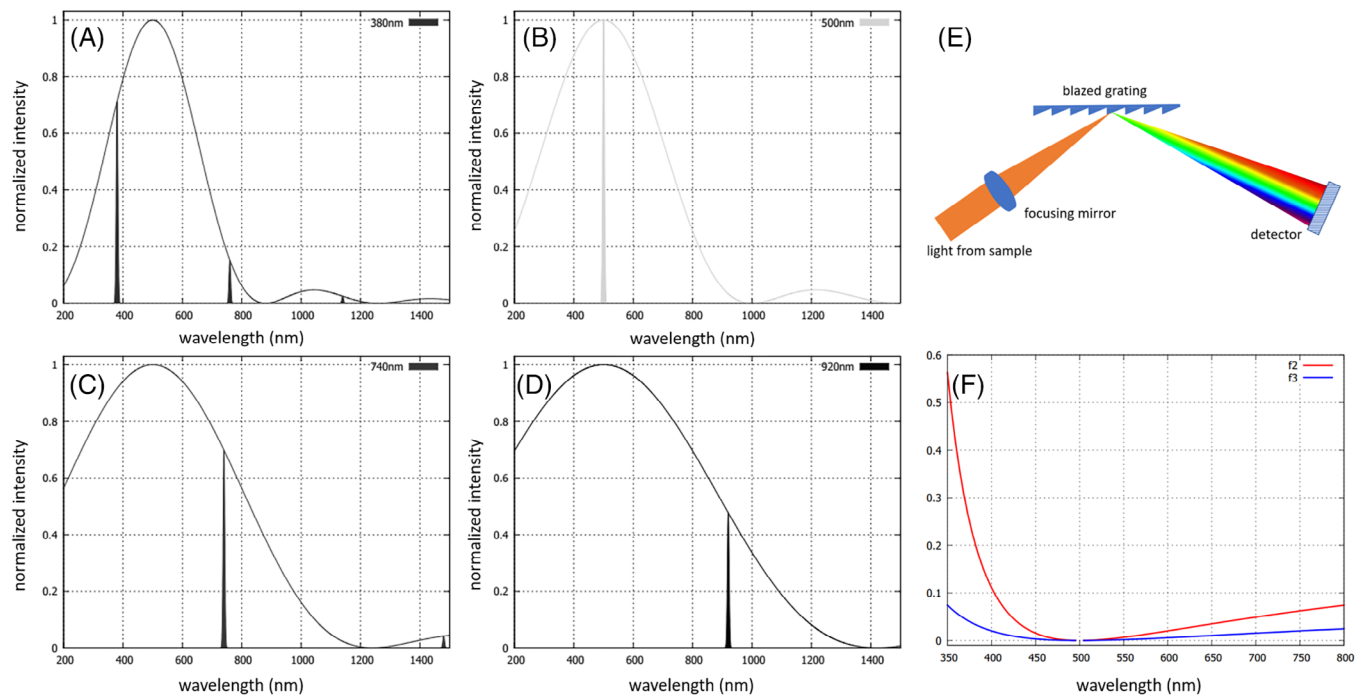


FIGURE 5 Spectral shapes of monochromatic light reflected by a blazed grating optimised for 500 nm wavelength. The x-axis is the wavelength but can be understood as the position where the reflected and diffracted light hits the detector. Thus, (A) light of 380 nm can also be found at the position of 760 nm, (B) light of 500 nm can only be found at the position of 500 nm, (C) light of 740 nm is also detected at 1480 nm and (D) light of 920 nm has no second maximum in the accessible range. A sketch of the grating is shown in (E) and (F) gives the correction functions for second- and third-order diffraction.

where $R(\lambda)$ is the reflection coefficient of the mirrors in the spectrometer set-up, l is the length of the optical light guides leading the light from the sample to the spectrometer and $DQE(\lambda)$ is the detection quantum efficiency of the detector and the last factor containing the sum is the original spectrum up to the third order of refraction. I_m denotes the intensity in the m th order. Higher orders are not accessible with our system. Hence, higher-order refraction has to be considered prior to any correction for the system components, such as the optical fibres and the CCD detector.

The correction has to take into account the intensity ratio between the first and m th diffraction order. Thus, a correction function f_m can be defined

$$f_m = \frac{\text{sinc}^2\left(\frac{\lambda_B}{\lambda} - m\right)}{\text{sinc}^2\left(\frac{\lambda_B}{\lambda} - 1\right)},$$

where the denominator is the efficiency for the first-order diffraction and the counter is the one for the m th order. In Figure 5F, the correction functions for $m = 2$ and $m = 3$ are shown.

Employing the correction functions eliminates higher-order refraction as shown in Figure 6. There the CL

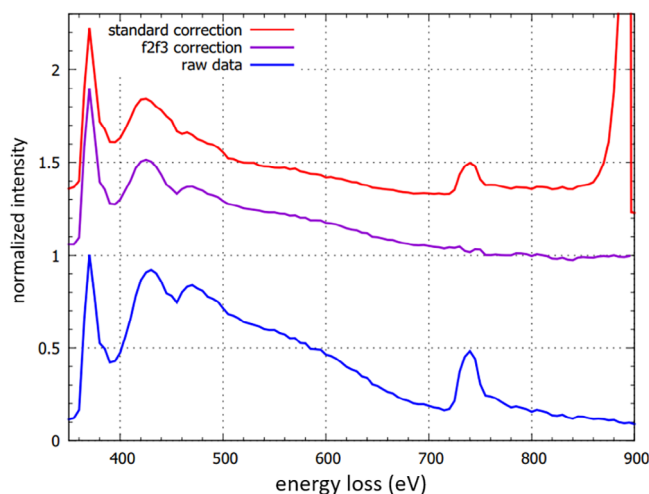


FIGURE 6 CL spectrum of GaN: bottom – raw data, centre – after correction for higher orders and spectrometer response, and top – correction only for the spectrometer response, ignoring higher order of refraction.

spectrum of GaN is shown as recorded (bottom), being corrected by the standard routine (top). Both of these spectra show a prominent peak at 740 nm, which would lead to an interpretation that the investigated GaN sample has a

strong red emission band in the band gap. When applying the correction function, this spurious signal is eliminated.

2 | CONCLUSION

In the present review, we described several aspects of the investigations of optical properties of semiconductors by employing electron beam techniques. We showed that the spatial resolution is limited by the inelastic delocalisation, which can be overcome, when working under dark-field conditions. This can be achieved by using a Bessel beam illumination, conical dark-field or energy filtered dark-field STEM. Another advantage of dark-field conditions is that Čerenkov losses are not detected. When using CL, the Čerenkov effect has to be avoided, since strong interference effects might appear. By the reduction of the beam energy, this effect can totally be suppressed and beam damage is avoided additionally.

Finally, we discussed the correct interpretation of CL spectra under consideration of the diffraction effects in the analysing grating. We demonstrated that higher-order refraction of the analysing grating has to be considered during the correction routine for the spectrometer response.

ACKNOWLEDGEMENTS

This research was in part supported by the SINNCE project of the European Union's Horizon 2020 program under the grant agreement No. 810626 and by the Austrian Research Promotion Agency, grant agreement Nr. 1110-00070.

ORCID

Michael Stöger-Pollach  <https://orcid.org/0000-0002-5450-4621>

REFERENCES

- Howie, A. (2003). Valence excitations in electron microscopy: Resolved and unresolved issues. *Micron*, *34*, 121–125.
- Muller, D. A., & Silcox, J. (1995). Delocalization in inelastic scattering. *Ultramicroscopy*, *59*, 195–213.
- Egerton, R. F. (2013). Control of radiation damage in the TEM. *Ultramicroscopy*, *127*, 100–108.
- Stöger-Pollach, M., Franco, H., Schattschneider, P., Lazar, S., Schaffer, B., Grogger, W., & Zandbergen, H. W. (2006). Čerenkov losses: A limit for bandgap determination and Kramers–Kronig analysis. *Micron*, *37*, 396–402.
- Horák, M., & Stöger-Pollach, M. (2015). The Čerenkov limit of Si, GaAs and GaP in electron energy loss spectrometry. *Ultramicroscopy*, *157*, 73–79.
- Stöger-Pollach, M., Löffler, S., Maurer, N., & Bukvišová, K. (2020). Using Čerenkov radiation for measuring the refractive index in thick samples by interferometric cathodoluminescence. *Ultramicroscopy*, *214*, 113011.
- Stöger-Pollach, M., Pichler, C. F., Dan, T., Zickler, G. A., Bukvišová, K., Eibl, O., & Brandstätter, F. (2021). Coherent light emission in cathodoluminescence when using GaAs in a scanning (transmission) electron microscope. *Ultramicroscopy*, *224*, 113260.
- Stöger-Pollach, M., Bukvišová, K., Schwarz, S., Kvapil, M., Šamořil, T., & Horák, M. (2019). Fundamentals of cathodoluminescence in a STEM: The impact of sample geometry and electron beam energy on light emission of semiconductors. *Ultramicroscopy*, *200*, 111–124.
- Swanson, G. J. (1989). Binary optics technology: The theory and design of multi-level diffractive optical elements. *Technical Report*, *854*, 1–53.
- Bohr, N. (1913). II. On the theory of the decrease of velocity of moving electrified particles on passing through matter. *Philosophical Magazine*, *25*, 10–31.
- Kohl, H., & Rose, H. (1985). Theory of Image Formation by Inelastically Scattered Electrons in the Electron Microscope. In: P. W. Hawkes, *Advances in electronics and electron physics* (Vol. 65, pp. 173–227). France: Laboratoire d'Optique Electronique du Centre National de la Recherche Scientifique Toulouse.
- Gu, L., Srot, V., Sigle, W., Koch, C., & Aken, P. A. (2008). VEELS band gap measurements using monochromated electrons. *Journal of Physics: Conference Series*, *126*, 012005.
- Stöger-Pollach, M., Schachinger, T., Biedermann, K., & Beyer, V. (2017). Valence EELS below the limit of inelastic delocalization using conical dark field EFTEM or Bessel beams. *Ultramicroscopy*, *174*, 24–30.
- Palik, E. D. (1985). *Handbook of optical constants of solids*. Orlando, FL, USA: Academic Press.
- Stöger-Pollach, M. (2008). Optical properties and bandgaps from low loss EELS: Pitfalls and solutions. *Micron*, *39*, 1092–1110.
- Griffiths, J. T., Zhang, S., Lhuillier, J., Zhu, D., Fu, W. Y., Howkins, A., Boyd, I., Stowe, D., Wallis, D. J., Humphreys, C. J., & Oliver, R. A. (2016). Nano-cathodoluminescence reveals the effect of electron damage on the optical properties of nitride optoelectronics and the damage threshold. *Journal of Applied Physics*, *120*, 165704.
- Stoddard, N., Duscher, G., Windl, W., & Rozgonyi, G. (2005). A new understanding of near-threshold damage for 200 keV irradiation in silicon. *Journal of Materials Science*, *40*, 3639–3650.
- Spencer, M. G., & Alam, T. (2019). High power direct energy conversion by nuclear batteries. *Applied Physical Review*, *6*, 031305.
- Okuno, Y., Okuda, S., Akiyoshi, M., Oka, T., Harumoto, M., Omura, K., Kawakita, S., Imaizumi, M., Messenger, S. R., Lee, K. H., & Yamaguchi, M. (2017). Radiation degradation prediction for InGaP solar cells by using appropriate estimation method for displacement threshold energy. *Journal of Applied Physics*, *122*, 114901.
- Stöger-Pollach, M., Laister, A., & Schattschneider, P. (2008). Treating retardation effects in valence EELS spectra for Kramers–Kronig analysis. *Ultramicroscopy*, *108*, 439–444.
- Yamamoto, N., Araya, K., Toda, A., & Sugiyama, H. (2001). Light emission from surfaces, thin films and particles induced by

- high-energy electron beam. *Surface and Interface Analysis*, 31, 79–86.
22. Kröger, E. (1968). Berechnung der Energieverluste schneller Elektronen in dünnen Schichten mit Retardierung. *Zeitschrift für Physik*, 216, 115–135.
 23. Stöger-Pollach, M., Zenz, K., Ursin, F., Schilberg, J., & Stöger, L. (2023). A correction for higher-order refraction in cathodoluminescence spectrometry. *Ultramicroscopy*, 251, 113770.

How to cite this article: Stöger-Pollach, M., Bukvišova, K., Zenz, K., Stöger, L., & Scales, Z. (2023). Important aspects of investigating optical excitations in semiconductors using a scanning transmission electron microscope. *Journal of Microscopy*, 1–8. <https://doi.org/10.1111/jmi.13242>